Auger and radiative filling rates of highly charged ions below metal surfaces

R. Díez Muiño and A. Salin
Laboratoire de Physico-Chimie Théorique, Université de Bordeaux I, URA 503 du CNRS, 351 Cours de la Libération, 33405 Talence Cedex, France
and Departamento de Física de Materiales, Universidad del País Vasco, Euskal Herriko Unibertsitatea, Apartado 1072, 20080 Donostia, Euskadi, Spain

N. Stolterfoht
Hahn-Meitner-Institut, Glienicker Straße 100, D-14109 Berlin, Federal Republic of Germany

A. Arnau and P. M. Echenique
Departamento de Física de Materiales, Universidad del País Vasco, Euskal Herriko Unibertsitatea, Apartado 1072, 20080 Donostia, Euskadi, Spain

(Received 24 April 1997; revised manuscript received 21 October 1997)

We evaluate quantitatively the role of Auger and radiative recombination processes in the neutralization of slow multicharged ions in metals. The strong perturbation of the valence-band electrons by the ion requires a nonlinear treatment which is carried out using density functional theory. We find that this perturbation creates an electronic cloud around the ion which has an atomiclike character. We show that it is this phenomenon which determines the order of magnitude of the transition rates, as illustrated by the evaluation of Auger and radiative rates for Ne and Ar ions. [S1050-2947(98)06902-9]

PACS number(s): 79.20.Rf, 73.90.+f, 78.70.−g

I. INTRODUCTION

Various processes have been proposed for the neutralization of slow multicharged ions traveling through metals [1]. Quasiresonant capture from metal core levels and Auger transitions are the more effective ones in filling the ion inner shells. Radiative recombination becomes also relevant for increasing transition energies (i.e., increasing ion charges). Quasiresonant capture has been studied both theoretically and experimentally in the last few years [2,3]. In this work we focus our attention on Auger and radiative transitions. The latter processes are directly related to experimental observables (electron and x-ray spectra). Furthermore, the neutralization and relaxation time scale determines the depth at which the potential energy of the incoming ion is deposited.

As the ion approaches and enters the solid, the metal is strongly polarized. The valence-band electrons are much affected by the ion perturbation and rapidly rearrange to *screen* the long-range Coulomb potential of the ion, ensuring charge neutrality at large distances. The time scale over which this rearrangement takes place is much smaller than the neutralization time. On the one hand, this reduction in the range of the electron-ion interaction potential makes the number of bound states on the ion finite. On the other hand, the charge cloud accumulated around the ion and following its motion corresponds to a modification of the electronic state of the metal in that region of space which is crucial for the determination of recombination processes.

Still, until now, theoretical studies dedicated to Auger processes taking place inside metals have been based on linear response theory [4–6]. The monoelectronic wave functions defining the initial and final states in a given transition were plane waves (or orthogonalized-plane waves) for the continuum states and hydrogenic wave functions for the bound states. The influence of screening on the latter was only included through an effective charge [4]. This approach has proved very successful in estimating the charge states of light projectiles in metals at velocities larger than the Fermi velocity of the medium [5].

However, a slow highly charged ion strongly perturbs a metal. The piling up of charge in the vicinity of the ion, particularly in the spatial region within a few atomic units around the nucleus, requires a nonlinear description of the electronic state modification. In this work we use density functional theory to obtain the induced electronic density around the ion self-consistently. The bound and continuum Kohn-Sham orbitals thus account for the charge displacement and significantly differ from the simpler approximations already mentioned. By using the latter orbitals in the calculation of Auger and radiative transition rates, we are able to account for target distortion in the evaluation of neutralization processes.

In addition to its intrinsic theoretical interest, the field is now very active from the experimental point of view. In the last few years, measurements on slow highly charged ions interacting with surfaces have brought a wealth of information on x-ray emission [7–9] and slow and fast electron emission spectra [10–12]. Following the works of Meyer *et al.* [13,14] and Burgdörfer *et al.* [15], it is now commonly accepted that Auger electrons mainly come from below the surface. The existence of an image-charge acceleration limits the available interaction time above the surface which avoids total neutralization and relaxation of the ion before entering the solid, even for projectile energies as low as a few hundred eV [16]. For a detailed understanding of the collision dynamics of the system, it is necessary to know the time scales of the radiative and nonradiative processes. However, their rates are not directly accessible experimentally. There-

fore, in the interpretation of experimental spectra, they are usually taken from calculations for isolated atoms [17,18] or used as fitting parameters in cascade models [13,14]. Our objective is to provide theoretical values that may be used as input to the cascade models. As will be shown, these rates may be in error by orders of magnitude when target distortion by the projectile is not accounted for.

A brief account of some of our results has already been reported [19].

Atomic units are used throughout unless otherwise stated.

II. THEORETICAL MODEL

A. Description of the system highly charged ion metal

Density functional theory (DFT) has successfully been used in the description of the nonlinear screening effects associated with the interaction of slow multicharged ions with metals [20], as well as in the calculation of molecular orbitals formed in the collision of a highly charged ion with a target atom in a metal [2]. The starting point is the DFT formalism as applied to a static impurity of charge Z_1 embedded in a free electron gas (FEG) of mean density n_0 [21,22] [we define the parameter r_s from $1/n_0=(4/3)\pi r_s^3$]. The static approximation is appropriate for ion velocities well below the Bohr velocity [6]. Although, in principle, the basic formulation of DFT is only rigorously founded for the ground state of the system, the method has proven to be useful in the estimation of excited-state energies [23], as in the case of a highly charged ion with some inner-shell vacancies. Furthermore, several authors [23,24] have argued that, when the lifetime of one of these excited states is long enough, the system can be considered as a subspace of the total Hamiltonian with a well-defined symmetry and orthogonal to the complementary space. This would mean that a local minimum in the energy functional giving the excited-state total energy does exist.

The basis of the Kohn-Sham approach is to solve iteratively, in a self-consistent way, the one-electron equations [25]:

$$\left\{-\frac{1}{2}\nabla^2+v_{\rm eff}[n]\right\}\phi_i=\epsilon_i\phi_i\,, \tag{1}$$

where the effective potential $v_{\rm eff}$ is composed of

$$v_{\rm eff}=v_{\rm ext}+v_{\rm ind}+v_{\rm xc}\,, \tag{2}$$

with

$$v_{\rm ext}=-\frac{Z_1}{r}, \tag{3}$$

$$v_{\rm ind}=\int d\mathbf{r}'\frac{n(r')}{|\mathbf{r}-\mathbf{r}'|}, \tag{4}$$

and $v_{\rm xc}$ is the exchange and correlation potential, that is obtained in the local density approximation (LDA) [26].

The electronic density $n(r)$ is obtained from the sum over occupied states:

$$n(r)=\sum_{i\in\,\rm occ}|\phi_i|^2. \tag{5}$$

This sum includes a contribution originating from the occupied bound states and another one coming from the integration over the continuum up to the Fermi level. For open L-shell configurations, a spherical average is performed.

The total energy for each L-shell configuration is obtained as the sum of three terms: the kinetic energy T, the electrostatic energy $E_{\rm es}$, and the exchange and correlation energy $E_{\rm xc}$:

$$T=\sum_i\,\epsilon_i-\int d\mathbf{r}\;n(r)v_{\rm eff}(\mathbf{r}), \tag{6}$$

$$E_{\rm es}=\int d\mathbf{r}\;n(r)\left\{v_{\rm ext}(r)+\frac{1}{2}\int d\mathbf{r}'\frac{n(r')}{|\mathbf{r}-\mathbf{r}'|}\right\}, \tag{7}$$

$$E_{\rm xc}=\int d\mathbf{r}\;n(r)\epsilon_{\rm xc}[n(r)], \tag{8}$$

where $\epsilon_{\rm xc}[n(r)]$ is the exchange and correlation energy density.

To obtain the transition energy between two different electronic configurations of the ion, we subtract the total energies of the final and initial states. In the processes under study, this energy transfer is balanced by the emission of a photon or an Auger electron.

Kohn-Sham equations allow us to determine the perturbed potential created by the ion and the electronic density around it. However, as our goal is to determine the transition rates, we need another level of approximation: the use of the Kohn-Sham orbitals as our monoelectronic wave functions. Accordingly, for a given electronic configuration, we fix a number n_h of empty orbitals when solving iteratively the set of equations (1). This leads to a generalization of Friedel sum rule [27] from the charge neutrality of the system:

$$Z_1+n_h=\frac{2}{\pi}\sum_l\,(2l+1)\,\delta_l(k_F), \tag{9}$$

where $\delta_l(k_F)$ is the scattering phase shift at the Fermi level. The addition of n_h to Z_1 in Eq. (9) accounts for the lack of n_h electrons in the empty bound states. To conserve the long-distance charge neutrality of the system, the number of occupied continuum states increases to compensate for the presence of n_h holes.

The number of holes n_h not only determines the total number of electronic states, but also how many of them are bound. As n_h decreases, the outer bound orbitals merge into the continuum, without appreciably varying their spatial shape. This means that the screening by a low-lying orbital in the continuum is very similar to that of a weakly bound state. In order to see this more clearly, it is useful to study the total change in the density of states induced by the ion in the continuum, defined as

$$\delta\rho(k)=\frac{2}{\pi}\sum_l\,(2l+1)\,\frac{d}{dk}\,\delta_l(k), \tag{10}$$

and its angular momentum components.

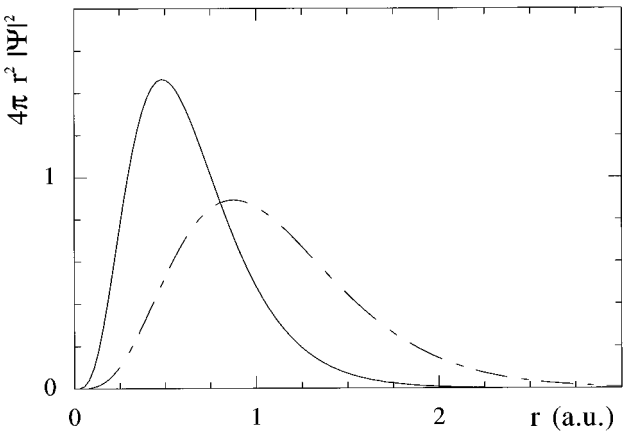

FIG. 1. Electronic charge density associated with the Kohn-Sham $2p$ orbital for the $1s^1 2s^2 2p^2$ configuration of a Ne^{5+} ion embedded in a free electron gas with $r_s = 2.0$ (solid line). The dashed line is the corresponding hydrogenic wave function for the same energy ω and an effective charge $Z_{\text{eff}} = (-2n^2\omega)^{1/2}$ (n is the principal quantum number).

The nonlinear screening produced by the valence electrons and the corresponding shortening of the range of the Coulomb potential strongly affects the shape of the one-electron wave functions (except, obviously, for deeply bound orbitals). As an example of this, we plot in Fig. 1 the wave functions for the $2p$ orbital of a Ne^{5+} ($1s^1 2s^2 2p^2$) ion in a FEG with $r_s = 2.0$ a.u. calculated within the DFT formalism, and the corresponding hydrogenic wave functions with the same energy. As the Auger rates are fairly sensitive to the shape of the bound-state wave functions [6], the results of Fig. 1 prove the importance of accounting for the target distortion in their definition.

B. Auger processes

In this work we study two types of Auger processes: *capture* and *intra-atomic* Auger processes. They are schematically depicted in Fig. 2. Both types involve an excitation in the valence band of the metal and *not* the emission of an electron already bound to the ion. We disregard atomiclike transitions such as the KLL or KLM ones.

In the *capture* process, an electron decays from a continuum state in conjunction with an individual (electron-hole pair) or collective (plasmon-type) excitation in the valence band of the metal. This transition changes the charge state of the ion. On the other hand, we call *intra-atomic* those processes in which the electron decays from a bound state of the ion while creating an excitation in the valence band. In this case, the ion charge state does not change, but only the electronic configuration of the ion.

We follow the standard notation in atomic Auger spectroscopy, but due to the fact that we treat the initial continuum state in the capture process (eigenstate of the Hamiltonian including the solid-state self-consistent DFT potential) different from the electronic excitations created in the metallic medium (modeled by a response function built from extended valence-band states), they are, respectively, denoted as C and V states. For example, an LCV process is a process in which the final localized state (L) belongs to the

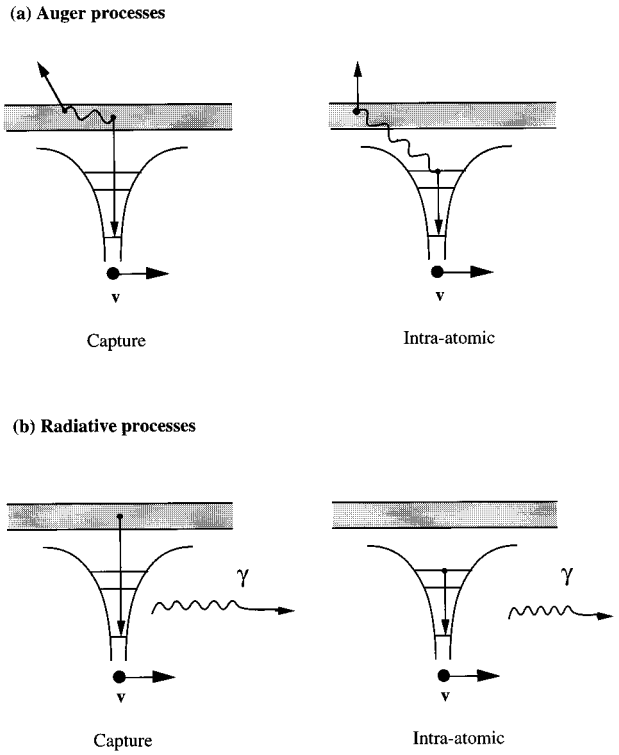

FIG. 2. Diagram of the (a) Auger and (b) radiative processes studied in this work. In a capture process an electron decays from the valence band of the metal to a bound state of the ion while creating either an electronic excitation (Auger) or emitting a photon (radiative). In an intra-atomic process, the electron decays from a bound state of the ion to one of lower energy.

L shell of the ion, the initial continuum electronic state (C) is centered at the ion, and the electronic excitation (V) involves unperturbed valence-electron states [19].

Within the dielectric formalism, the probability of an Auger transition induced by the screened Coulomb interaction between the electrons can be obtained from the imaginary part of the self-energy associated with the state [4], i.e., a magnitude related to its lifetime. Alternatively, one can use first-order time-dependent perturbation theory to calculate the transition rates between two states of the many-body problem [5]. In both cases, the Auger rate per unit time and per spin state in the capture process can be expressed as

$$\Gamma_i^A = 4 \sum_{k<k_F} \int d\omega \int \frac{d^3\mathbf{q}}{q^4} |\langle \phi_i | e^{i\mathbf{qr}} | \phi_k \rangle|^2 S(\mathbf{q},\omega)\, \delta(\omega - \Delta E). \tag{11}$$

Here, k_F is the Fermi wave number and $|\phi_k\rangle$, $|\phi_i\rangle$ are, respectively, the initial continuum and the final bound one-electron states. As the Hamiltonians defining the latter are different for the initial and final electronic configurations, the state $|\phi_i\rangle$ is not orthogonal to the continuum states $|\phi_k\rangle$. However, we have checked that the term $q = 0$ gives a negligible contribution to the integral of Eq. (11) in the systems under study. Hence the lack of orthogonality between the initial and final wave functions does not artificially increase the value of the rates. The dynamic structure factor $S(\mathbf{q},\omega)$ accounts for the medium response and measures the density of excitations in the FEG. We will use in this work the wave-

vector- and frequency-dependent random-phase approximation (RPA) to this function [28]. That means that the excitations created in the metal are described by unperturbed plane waves, from which the RPA response function is built. This can be justified considering that the valence-band excitations are extended all along the metal.

The one-electron matrix elements in Eq. (11) depend on the overlap between the initial and final states. The sum over occupied states up to the Fermi level introduces the dependence of the rates on the unperturbed electronic density of the metal, n_0. The transition energy ΔE, entering the argument of the response function, weights the probability of creating an excitation in the valence band of the metal with this fixed energy.

In the case of intra-atomic processes, the expression for the Auger transition probability is the same except that the initial state is a bound state on the ion, $|\phi_j\rangle$, and the sum over momenta k disappears.

C. Radiative transitions

In the same way as we have treated the Auger transitions, we will distinguish between radiative processes that change the charge state of the ion and those that modify its electronic configuration (Fig. 2). We denote *radiative capture* processes those processes in which the initial state of the electron is a continuum state centered at the ion. *Radiative intra-atomic* processes are those processes in which both the initial and final state of the electron are bound states of the ion.

In this work, we limit ourselves to the dipole approximation. The probability per unit time and per spin state, summed over all polarizations, for radiative capture is given by

$$\Gamma_i^r = \sum_{k<k_F} \frac{4\alpha}{3c^2}(\Delta E)^3 |\langle \phi_k|\mathbf{r}|\phi_i\rangle|^2. \tag{12}$$

Here α is the fine structure constant and c is the speed of light. The states $|\phi_i\rangle$ and $|\phi_k\rangle$ are defined in the same way as in the case of Auger transitions. Although the cubic factor in the transition energy is not responsible for the whole dependence on the transition energy (the dipolar matrix elements usually increase when the transition energy decreases) it is an indication that radiative transitions will play a prominent role for heavy ions. The modifications of this expression in the case of radiative intra-atomic processes are the same as in the Auger formalism: the initial state is a bound state, $|\phi_j\rangle$, and the sum up to the Fermi level disappears.

To obtain the radiative transition probabilities, we will use the same one-electron wave functions as in the Auger calculations to account for the perturbation induced by the ion in the medium, i.e., the eigenstates of the Hamiltonian including the self-consistent DFT potential.

III. RESULTS AND DISCUSSION

A. Highly charged Ne ions in metals

To establish a connection with experiment [12,29] we assume that the Ne ion has one K-shell electron. We also assume that, once the ion has entered the solid, its M shell (if bound) is rapidly filled. Then, the ion has some inner-shell holes (one K-shell hole and a given number of L-shell holes) and an electronic screening cloud surrounding it, composed of a continuum contribution and occasionally of a bound contribution originating from the M shell. This negatively charged cloud completely screens the ion at large distances. The quantities that determine whether the M shell is bound or not are the electronic background density of the FEG, n_0, and the number of electrons in the inner shells. In the case of a Ne ion with one K-shell hole inside a FEG with $r_s=1.5$ (corresponding to Au) [30], the M shell is never bound, regardless of the number n_L of L-shell electrons. However, when the electronic density parameter r_s is equal to 2.0 (Al) [30], the $3s$ orbital is bound if $n_L \leqslant 5$. This is shown in Fig. 3 where we plot the total radial density, as well as the contributions to it. The data refer to a Ne ion with various electronic configurations in a FEG with $r_s=2.0$.

As n_L increases, the screening cloud extends around the ion. This cloud has an M-shell character and, accordingly, the induced electronic density looks like that of a neutral Ne atom with the same number of inner-shell holes. In a more general way, we can state that the induced screening cloud around the ion mimics the charge distribution of the isolated atom shell next to the one in which the vacancies are [2,3]. As an example of this we plot in Fig. 4 the induced electronic density around a Ne^{9+} ion in a FEG for two different values of the background density. We compare it with a Hartree-Fock-Slater calculation of the electronic density around a neutral Ne atom in an excited state and with the same number of holes in the K and L shells. The electronic density is quite similar in the three cases, except for the long-range Friedel oscillations of the screened potential inside the solid. Furthermore, a characteristic feature of the ion-solid system is that the total density can be smaller than the background density at large distances (overscreening).

For $r_s=2$ and when $n_L>5$, the $3s$ orbital merges into the continuum and the screening cloud no longer has a bound contribution. This modification does not affect much the shape of the electronic cloud, as shown in Fig. 3. It may be better understood with the help of Fig. 5, in which we present the induced density of states in the continuum and its angular momentum, as defined in Eq. (10), for a given L-shell configuration. The contribution of each continuum l component depends strongly on the existence of a bound state with the same value of l. This is shown, for example, by the sudden appearance of a low-energy peak in the s-wave curve when a sixth electron is deposited into the L shell. This peak corresponds to the merging of the $3s$ orbital into the continuum, as mentioned before. On the other hand, the main components of the screening density are the p wave and the d wave. The first one is favored only when few electrons populate the bound $2p$ orbital and the second one when the core shells are nearly filled and the screening cloud radius extends up to 3–4 a.u.

We plot in Fig. 6 the total L-shell Auger filling rate, Γ_L^A, for Ne ions in a FEG of $r_s=1.5$ and $r_s=2.0$, as a function of the initial number of electrons in the L shell. In the case of $r_s=2.0$, the rate is the sum of the LCV and the LMV rates ($\Gamma_L^A=\Gamma_{LCV}^A+\Gamma_{LMV}^A$), the latter being nonzero only when $n_L \leqslant 5$. However, for $r_s=1.5$, the Auger rate Γ_L^A is equal to

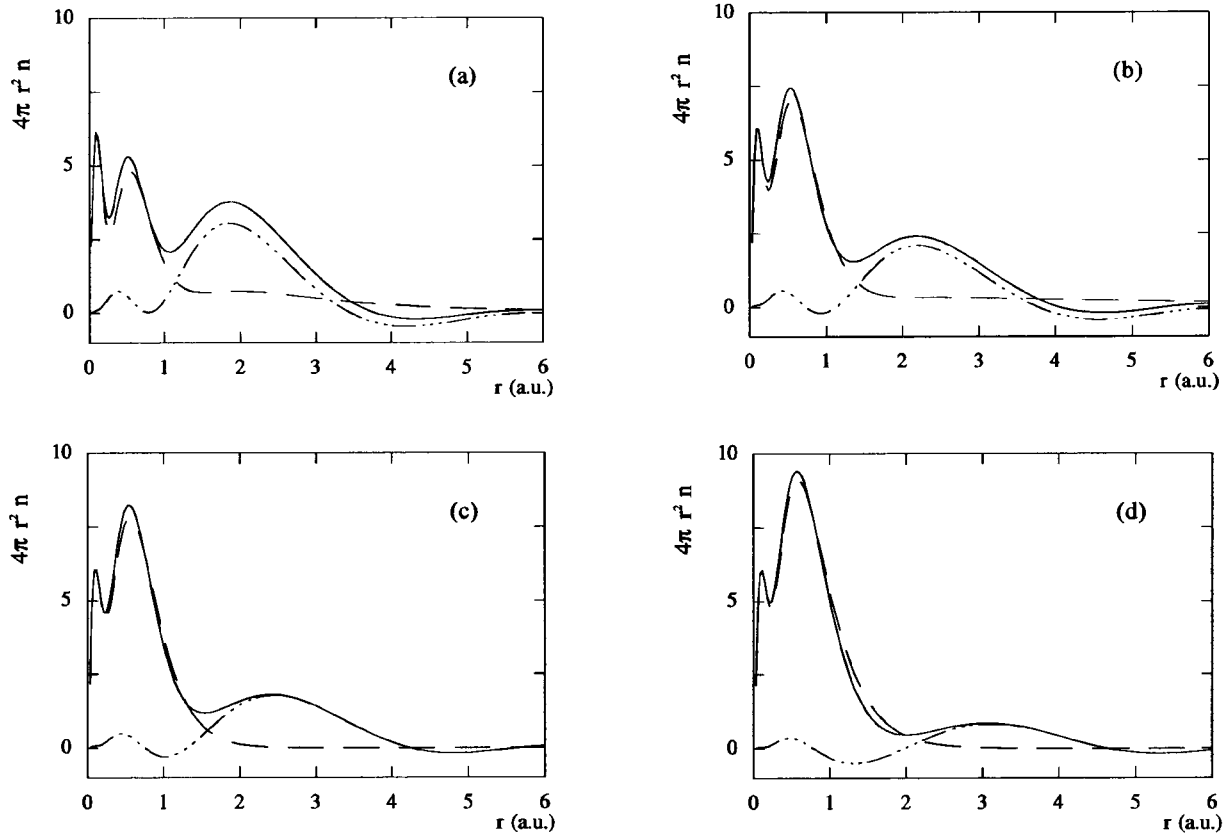

FIG. 3. Radial dependence of the induced electronic density around a Ne ion with four different electronic configurations in a free electron gas ($r_s=2.0$): (a) $1s^1 2s^2 2p^1$, (b) $1s^1 2s^2 2p^3$, (c) $1s^1 2s^2 2p^4$, and (d) $1s^1 2s^2 2p^6$. The solid line is the total density decomposed into two contributions: the component from the K and L bound shells (dashed line) and the screening component coming from the M shell orbitals (if bound) and the continuum orbitals (dash-dotted line).

Γ^A_{LCV}, as the M shell is never bound.

The L-shell filling rates of Ne atoms are weakly dependent on the number of electrons in the L shell. This is due to the compensation of two effects: on the one hand the number of available final states enhances the total rate when n_L is small. On the other hand the rate per spin state increases with n_L as the overlap between the initial and final orbitals is larger and the transition energy ΔE lower. It should be noted that this behavior is not general. If ΔE becomes smaller than the plasmon energy of the metal, excitation of collective modes in the medium is inhibited and the transition rates appreciably decrease. This is the case for the L-shell filling rates of N ions in metals, as already shown in [19]. In the case of Ne, as can be seen in Fig. 7, the LCV transition energies are always above the plasmon peak, even for the largest values of n_L.

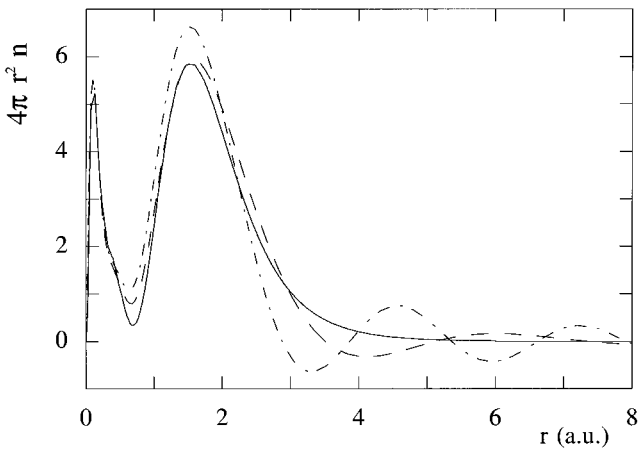

FIG. 4. Radial dependence of the induced electronic density around a Ne^{9+} ion ($1s^1$) for two different background electronic densities: $r_s=1.5$ (dash-dotted line) and $r_s=2.0$ (dashed line). The solid line represents the radial electronic density around a neutral isolated Ne atom in an excited state (Ne $1s^1 3s^2 3p^6 3d^1$), calculated as indicated in the text.

The variation of the rates with the background electronic density n_0 is linear when n_L is small and quadratic for a nearly filled L shell. To understand this dependence, one should have in mind that in the Auger capture process we are summing twice over the valence-band electrons: once when summing over all electrons decaying to the L shell and a second time when summing over possible excitations in the medium. In the latter case, our approach does not account for the distortion produced by the multicharged ion, so the dependence is always linear on n_0. However, in the sum over initial states in the decaying channel, the perturbation induced by the ion is stronger when the number of L-shell electrons is low. Defining the total continuum electronic density as $n=n_0+\Delta n$ (Δn being the density induced in the medium by the impurity), when the number of L-shell electrons is small the ion is highly charged and the induced den-

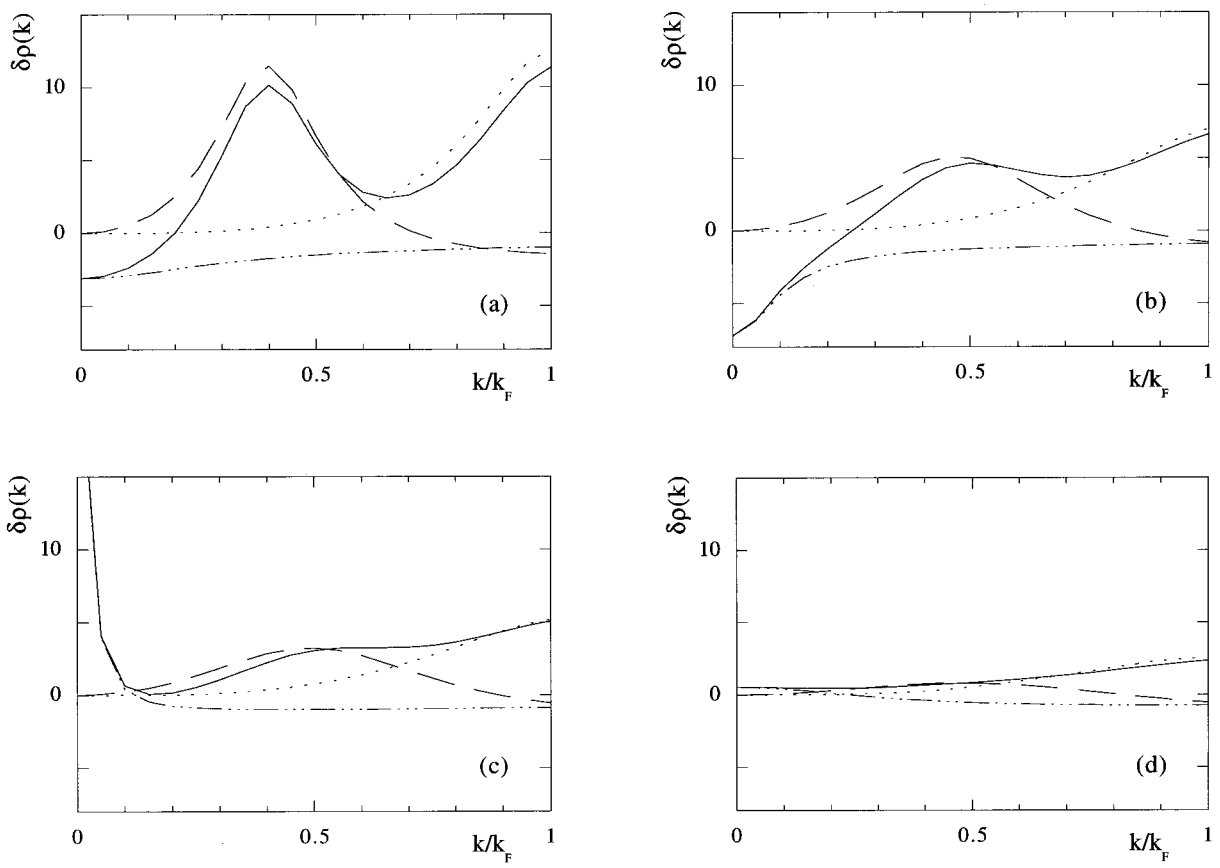

FIG. 5. Induced density of states in the continuum as defined in Eq. (10) for the same system and same configurations as in Fig. 3. The solid line is the total induced density, decomposed in its partial-wave components: *s* wave (dash-dotted line), *p* wave (dashed line), and *d* wave (dotted line). $\delta\rho(k)$ is plotted as a function of the linear momentum k in units of the Fermi momentum.

sity Δn is much larger than the background density n_0. Then, the dependence on n_0 originates mostly from the structure factor and the dependence of the rate on n_0 is linear. On the other hand, in the case of large n_L (the ion is nearly neutral), the background density is weakly perturbed and we have a stronger n_0 dependence of the rates caused by the sum over initial states. This gives rise to a total n_0^2 dependence.

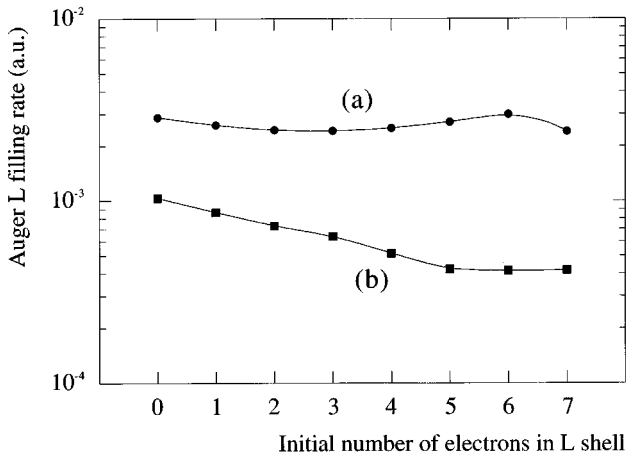

FIG. 6. L-shell Auger filling rates for a Ne ion in a free electron gas as a function of the initial number of electrons in the L shell: (a) $r_s=1.5$ ($\Gamma_L^A=\Gamma_{LCV}^A$); (b) $r_s=2.0$ ($\Gamma_L^A=\Gamma_{LCV}^A+\Gamma_{LMV}^A$).

As the L shell of the Ne ion inside the metal is being filled, the K-shell hole can be filled by KLV or KLL processes. In order to estimate how important these channels are in the evolution of the ion configuration, we plot in Fig. 8 the

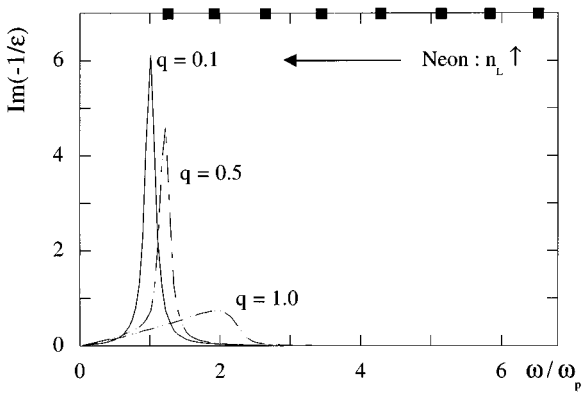

FIG. 7. ω dependence (in units of the plasmon frequency ω_p) of the imaginary part of the inverse dielectric function $[\mathrm{Im}(-1/\epsilon)]$ for three different q values in the case of a free electron gas with $r_s=2.0$. It is related to the structure factor $S(q,\omega)$ by the relation $\mathrm{Im}(-1/\epsilon)=(4\pi^2/q^2)S(q,\omega)$. The squares in the upper axis represent the theoretical LCV transition energies for Ne ions with $1\leqslant n_L\leqslant 8$. $\mathrm{Im}(-1/\epsilon)$ is essentially a monotonically decreasing function of ω as n_L decreases (ω increases).

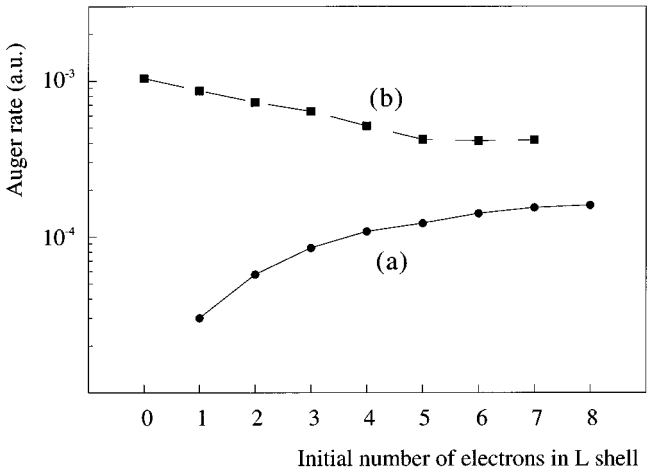

FIG. 8. (a) Auger KLV rate (Γ^A_{KLV}) for a Ne ion inside a free electron gas with $r_s=2.0$ as a function of the initial number of electrons in the L shell. Also plotted (b) is the total L-shell Auger rate ($\Gamma^A_L=\Gamma^A_{LCV}+\Gamma^A_{LMV}$).

KLV Auger rate, Γ^A_{KLV}, for Ne ions in Al, compared to the total Γ^A_L rate. Considering that the KLL process is even faster than the KLV one and that it increases with n_L [29], we can conclude that the probability of a Ne ion to completely fill its L shell before one of its electrons decays to the K shell is very small. A similar conclusion has been extracted from experimental measurements: Grether *et al.* [12] have estimated that, when the K hole is filled, the number of electrons in the L shell is $n_L \approx 2-3$. This conclusion is based on the observation of the KLL spectra at low projectile velocities, when quasiresonant capture can be neglected. The filling of the K-shell hole causes an acceleration of the L-shell filling process since it decreases the L-shell binding energy.

In a recent publication [3], Stolterfoht *et al.* have employed a multiple-cascade model to study the filling of the K and L vacancies of highly charged Ne ions impinging on Al targets. Accounting for the electron transport towards the surface, they are able to reproduce the main features of the experimental spectra, as the angular distribution of the emitted K Auger electrons, or the mean L-shell occupation number during the L and K Auger emission. In their analysis, they use an Auger L-shell filling rate per spin state of 6.7×10^{-4} a.u., extrapolated from atomic calculations. This value is of the same order of magnitude as our theoretical one.

Grether *et al.* [12] have used a similar model to fit the Auger Γ^A_{KLV} rate in the Ne/Al system, after fixing the rest of the transition rates and assuming no dependence of the Γ^A_{KLV} rate on the number of L-shell electrons. The fitted value $\Gamma^A_{KLV}=3\times10^{-3}$ a.u. is very close to our theoretical result, plotted in Fig. 8.

Auger rates obtained including the charge displacement in the medium contrast with former ones calculated under linear response theory [6]. These latter are roughly one order of magnitude lower and strongly dependent on the transition energies. The proximity of our results to the rates needed in the cascade models clearly shows the necessity of a nonlinear description of the ion-target interaction.

TABLE I. Transition energies (in eV) for the KL radiative process for an Ar ion inside a free electron gas ($r_s=1.97$) as a function of the initial number of electrons in the L shell. Our theoretical values are compared with the experiment [31].

n_L	ΔE (theor.)	ΔE (expt.)
3	3048.9	3057
4	3025.2	3040
5	3002.9	3016
6	2980.8	2994
7	2962.2	2975
8	2946.3	2955

The last comment on the L-shell filling in the Ne/Al case deals with neutralization processes that have not been included in our discussion. Radiative transitions are comparatively much less efficient due to the small transition energies involved. However, when the ion energy increases, quasiresonant capture can play an increasing role. On the other hand, Auger transitions may be crucial in opening this channel by bringing the L-shell energy levels into resonance with some target levels [2].

B. Highly charged Ar ions in metals

In the study of radiative transitions, we use the Ar ion as projectile rather than Ne because the transition energies are larger, implying larger radiative rates and hence fluorescence yields. Furthermore, the experimental x-ray spectra of Ar ions are much more complex than those of Ne. In the case of Ar with a K-shell hole inside a FEG with typical metallic r_s values, the $3s$ and $3p$ orbitals are bound. As a consequence, the screening cloud around the ion has always a bound component (assuming that the M shell is totally filled as we will consider in all the following) and the continuum component has a strong d-wave character.

The radiative processes filling the L shell of Ar are the LM and LC transitions, while the ones filling the K shell can be decomposed into KL, KM, and KC. The KL, KM, and LM processes essentially differ from the outside-the-solid situation in the modification of the ion electronic wave functions. KC and LC transitions are solid-state processes since the initial state in the transition is a target valence-band state. The inclusion of all possible radiative processes allows us to compare the total radiative yields into different shells.

One of the practical advantages of radiative spectra as compared to Auger measurements is that the attenuation length of photons inside a metal is much larger than for electrons. Hence, in order to compare experimental and calculated transition energies of the processes we are dealing with, it is more convenient to use radiative data. In Table I we give the calculated values for the transition energies in a KL radiative process (an electron decaying from the L to the K shell) for an Ar ion inside a FEG with $r_s=1.97$ (representing Si) [30] as a function of the initial number of electrons in the L shell. The theoretical transition energy is obtained as the difference between the total energies of the initial and final electronic configurations. The comparison with previous experimental data [31] shows that DFT gives fairly ac-

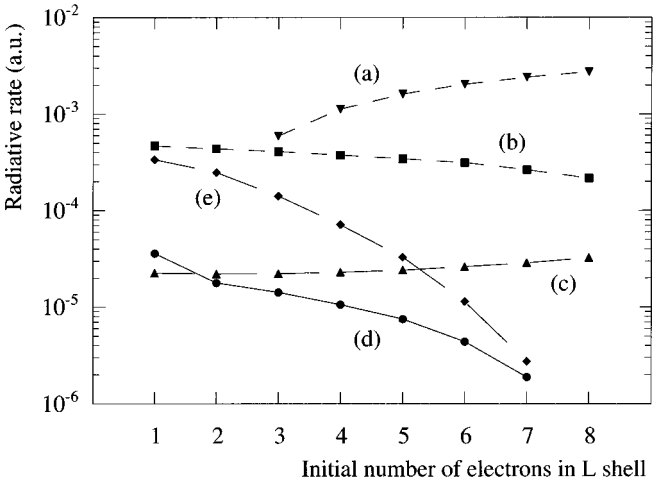

FIG. 9. K- and L-shell radiative filling rates for an Ar ion inside a free electron gas ($r_s=1.97$) as a function of the initial number of electrons in the L shell: (a) Γ^r_{KL}; (b) Γ^r_{KM}; (c) Γ^r_{KC}; (d) Γ^r_{LM}; (e) Γ^r_{LC}.

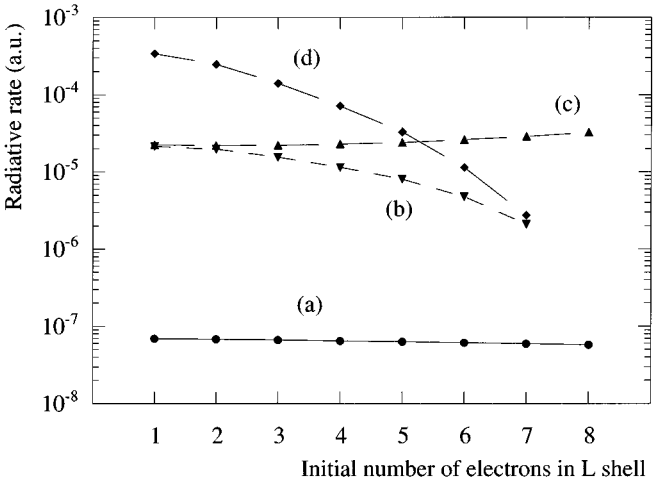

FIG. 10. Comparison between the KC and LC radiative rates of an Ar ion inside a free electron gas ($r_s=1.97$) as a function of the initial number of electrons in the L shell and using two different descriptions for the valence-band states: plane waves [(a) is the Γ^r_{KC} rate and (b) is the Γ^r_{LC} rate] or one-electron wave functions obtained from the DFT potential [(c) is the Γ^r_{KC} rate and (d) the Γ^r_{LC} one].

curate transition energies (the difference being lower than 1%).

Taking again the same system (Ar/Si), we plot in Fig. 9 the total rates Γ^r_K and Γ^r_L for all radiative processes filling the K and L shells of Ar ions with one initial K-shell hole as a function of the initial number of electrons in the L shell. As the Coster-Kronig-type $2p\rightarrow 2s$ transition is very fast, we consider that the electrons filling the L shell occupy the $2p$ orbital only after the $2s$ has been filled. This is why the KL process occurs only when $n_L>2$. This approximation agrees with the measurements which show very weak peaks for KL transitions when $n_L\leqslant 2$ [31].

Two competing factors determine the absolute values and the behavior of the radiative rates, i.e., the transition energy and the overlap between the final and initial wave functions. In the case of Ar/Si, the combination of both factors causes the KL transitions to be the fastest ones. The low value of the KC rates is a consequence of the strong d-wave character of the continuum states. In general, the total K-shell radiative rate Γ^r_K is higher than the total L-shell radiative rate Γ^r_L. However, when the number of L electrons is small they can be of the same order of magnitude (the transition energies are larger as well as the number of final states in the transitions to the L shell).

Once more, as in the case of Auger processes, the piling up of charge in the vicinity of the highly charged Ar ion determines the absolute values of the radiative capture rates. Its importance is well reflected in Fig. 10, in which we plot the Γ^r_{KC} and Γ^r_{LC} radiative rates as a function of the number of electrons in the L shell. The results are compared with those of a simpler model, in which the valence-band states are represented by plane waves, i.e., without the screening charge displacement around the ion. The two calculations differ by roughly one order of magnitude for the LC transitions and three orders of magnitude for the KC transitions.

Even if the relative importance of radiative processes increases with the nuclear charge of the ion, atomic calculations predict that an isolated Ar ion with K and/or L vacancies relaxes mainly by KLL and LMM Auger transitions [32,33]. We expect the same conclusion to hold in the metal since the L shell and the $3s$ and $3p$ orbitals of the M shell are bound. The KLL and LMM Auger rates cannot be obtained with the formalism developed in the present work, which is specifically devoted to processes including the collective effect of the valence-band electrons. Nevertheless, Auger processes in which the electronic excitation accompanying the decay is created in the valence band can also play a role. We plot in Fig. 11 the Auger KLV, LMV, and LCV rates for an Ar ion inside a FEG with $r_s=1.97$ as a function of the number of electrons in the L shell. Again, we consider

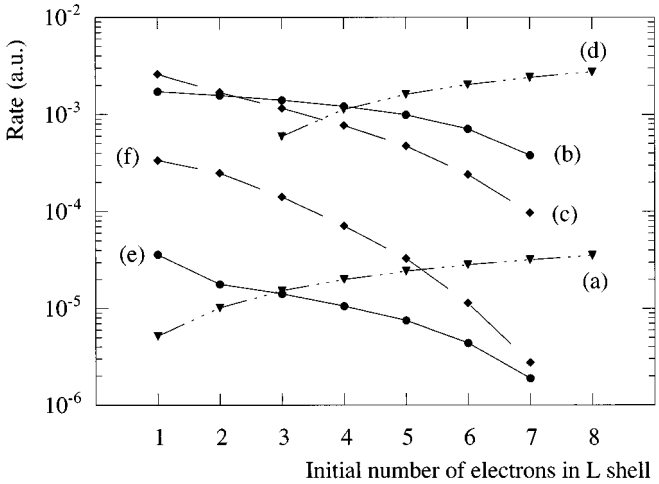

FIG. 11. K- and L-shell Auger rates for an Ar ion inside a free electron gas ($r_s=1.97$) as a function of the initial number of electrons in the L shell: (a) Γ^A_{KLV}; (b) Γ^A_{LMV}; (c) Γ^A_{LCV}. Some of the radiative rates presented in Fig. 9 are also plotted: (d) Γ^r_{KL}; (e) Γ^r_{LM}; (f) Γ^r_{LC}.

the ion with one K-shell hole and the M shell already filled. The Auger rates are compared with the corresponding KL, LM, and LC radiative rates. The KLV, KMV, and KCV rates are much smaller than the KL radiative widths (our results for the KMV and KCV rates are roughly of the same order of magnitude of the KLV rates plotted in Fig. 11). However, the opposite is true for the L shell: the sum of Γ^A_{LMV} and Γ^A_{LCV} is at least one order of magnitude larger than the total L-shell radiative rate.

IV. CONCLUSIONS

We have calculated absolute Auger and radiative transition rates for slow multicharged ions of Ne and Ar traveling in metals. Special attention has been paid to the strong perturbation of the valence-band electrons induced by the ion. The L Auger rates ($\Gamma^A_{LCV}+\Gamma^A_{LMV}$) we obtain for Ne roughly vary between 4×10^{-4} and 3×10^{-3} a.u. These values are of the same order of magnitude as those that can be obtained for isolated atoms (see, for example, the values quoted in Ref. [3]). The similarity of the calculated rates with the atomic case is not trivial. In fact, we obtain atomiclike rates *only* because the perturbation of the metal electrons by the ion charge produces a density cloud around the ion which has an atomiclike character. Calculations performed without target distortion [6] are nearly one order of magnitude smaller. The compatibility of our results with the experimental findings supports our claim that target distortion is essential to evaluate the neutralization rates of multicharged ions in metals.

For the case of Ar ions, the rates of Auger transitions involving a valence-band excitation are large for the decay of L holes and small for K holes, by comparison with the radiative widths. Our calculations of the radiative recombination rates for Ar ions show also the huge influence of the nonlinear valence-band distortion by the projectile charge.

ACKNOWLEDGMENTS

This work was partially supported by the Fonds Commun de Coopération Aquitaine–Euskadi (Conseil Régional d'Aquitaine–Eusko Jaurlaritza) and the Human Capital and Mobility program of the European Union under Contract No. CHRX-CT93-0103. One of us (R.D.M.) wishes to express thanks for the kind welcome of the Laboratoire de Physico-Chimie Théorique and acknowledges financial support by the Spanish Ministerio de Educación y Ciencia (Grant No. EX96-0050836672).

[1] For a review, see A. Arnau *et al.*, Surf. Sci. Rep. **27**, 113 (1997).
[2] A. Arnau, R. Köhrbrück, M. Grether, A. Spieler, and N. Stolterfoht, Phys. Rev. A **51**, R3399 (1995).
[3] N. Stolterfoht, A. Arnau, M. Grether, R. Köhrbrück, A. Spieler, R. Page, A. Saal, J. Thomaschewski, and J. Bleck-Neuhaus, Phys. Rev. A **52**, 445 (1995).
[4] F. Guinea, F. Flores, and P. M. Echenique, Phys. Rev. Lett. **47**, 604 (1982).
[5] P. M. Echenique, F. Flores, and R. H. Ritchie, in *Solid State Physics: Advances in Research and Applications*, edited by H. Ehrenreich and D. Turnbull (Academic, New York, 1990), Vol. 49, p. 230.
[6] R. Díez Muiño, A. Arnau, and P. M. Echenique, Nucl. Instrum. Methods Phys. Res. B **98**, 420 (1995).
[7] J.-P. Briand, L. de Billy, P. Charles, S. Essabaa, P. Briand, R. Geller, J. P. Desclaux, S. Bliman, and C. Ristori, Phys. Rev. Lett. **65**, 159 (1990).
[8] D. Schneider, M. A. Briere, J. W. McDonald, and J. Biersack, Radiat. Eff. Defects Solids **127**, 113 (1993).
[9] S. Ninoyima, Y. Yamazaki, K. Sawatari, M. Iruko, K. Komaki, T. Azuma, K. Kuroki, and M. Sekiguchi, Nucl. Instrum. Methods Phys. Res. B **115**, 177 (1996).
[10] J. Limburg, S. Schippers, R. Hoeckstra, R. Morgenstern, H. Kurz, F. Aumayr, and H. P. Winter, Phys. Rev. Lett. **75**, 217 (1995).
[11] F. Aumayr, H. Kurz, D. Schneider, M. A. Briere, J. W. McDonald, C. E. Cunningham, and H. P. Winter, Phys. Rev. Lett. **71**, 1943 (1993).
[12] M. Grether, A. Spieler, R. Köhrbrück, and N. Stolterfoht, Phys. Rev. A **52**, 426 (1995).
[13] F. W. Meyer, S. H. Overbury, C. C. Havener, P. A. Zeijlmans van Emmichoven, and D. M. Zehner, Phys. Rev. Lett. **67**, 723 (1991).
[14] F. W. Meyer, S. H. Overbury, C. C. Havener, P. A. Zeijlmans van Emmichoven, J. Burgdörfer, and D. M. Zehner, Phys. Rev. A **44**, 7214 (1991).
[15] J. Burgdörfer, P. Lerner, and F. W. Meyer, Phys. Rev. A **44**, 5674 (1991).
[16] R. Köhrbrück, N. Stolterfoht, S. Schippers, S. Hustedt, W. Heiland, D. Lecler, J. Kemmler, and J. Bleck-Neuhaus, Phys. Rev. A **48**, 3731 (1993).
[17] S. Schippers, J. Limburg, J. Das, R. Hoekstra, and R. Morgenstern, Phys. Rev. A **50**, 540 (1994); **50**, 4429(E) (1994).
[18] J. Limburg, J. Das, S. Schippers, R. Hoekstra, and R. Morgenstern, Surf. Sci. **313**, 355 (1994).
[19] R. Díez Muiño, N. Stolterfoht, A. Arnau, A. Salin, and P. M. Echenique, Phys. Rev. Lett. **76**, 4636 (1996).
[20] A. Arnau, P. A. Zeijlmans van Emmichoven, J. I. Juaristi, and E. Zaremba, Nucl. Instrum. Methods Phys. Res. B **100**, 279 (1995).
[21] E. Zaremba, L. M. Sander, H. B. Shore, and J. H. Rose, J. Phys. F **7**, 1763 (1977).
[22] P. M. Echenique, R. M. Nieminen, and R. H. Ritchie, Solid State Commun. **37**, 779 (1981).
[23] A. R. Williams and U. von Barth, in *Theory of the Inhomogeneous Electron Gas*, edited by S. Lundqvist and N. H. March (Plenum, New York, 1983), Chap. 4.
[24] R. M. Dreizler and E. K. Gross, *Density Functional Theory* (Springer-Verlag, Berlin, 1990).
[25] W. Kohn and L. J. Sham, Phys. Rev. **140**, A1133 (1965).
[26] O. Gunnarson and B. I. Lundqvist, Phys. Rev. B **13**, 4274 (1976).
[27] J. Friedel, Philos. Mag. **43**, 153 (1953).

[28] J. Lindhard, K. Dan. Vidensk. Selsk. Mat. Fys. Medd. **28**, 8 (1954).
[29] M. Grether, A. Arnau, R. Köhrbrück, A. Spieler, and N. Stolterfoht, Nucl. Instrum. Methods Phys. Res. B **115**, 157 (1996).
[30] D. Isaacson, *Compilation of r_s Values*, Radiation and Solid State Laboratory, New York University, internal report, 1975 (unpublished).
[31] J.-P. Briand, G. Giardino, G. Borsoni, M. Froment, M. Eddrief, C. Sébenne, S. Bardin, D. Schneider, J. Jin, H. Khemliche, Z. Xie, and M. Prior, Phys. Rev. A **54**, 4136 (1996).
[32] C. P. Bhalla, Phys. Rev. A **8**, 2877 (1973).
[33] N. Vaeck and J. Hansen, J. Phys. B **28**, 3523 (1995).